Inorganic Chemistry

Two-Phase Synthesis of Colloidal Annular-Shaped Ce$_x$La$_{1-x}$CO$_3$OH Nanoarchitectures Assemblied from Small Particles and Their Thermal Conversion to Derived Mixed Oxides

Thanh-Dinh Nguyen, Cao-Thang Dinh, and Trong-On Do*

Department of Chemical Engineering, Laval University, Quebec G1K 7P4, Canada

Undoped and cerium doped LaCO$_3$OH annular-shaped nanoarchitectures with high specific surface area have been fabricated via the thermolysis of Ce$_x$La$_{1-x}$(oleate)$_3$ (x = 0−20 mol %) complexes in a toluene−water system containing *tert*-butylamine/oleylamine. The products exhibit 400 nm-sized monodisperse annular-shaped nanoarchitectures, which are constituted of 3−5 nm-sized primary particles. A possible mechanism of the reaction of Ce$_x$La$_{1-x}$-(oleate)$_3$ and *tert*-butylamine for the formation of annular-shaped Ce$_x$La$_{1-x}$CO$_3$OH nanoarchitectures is proposed. The thermal conversion of Ce$_x$La$_{1-x}$CO$_3$OH to Ce$_x$La$_{1-x}$(CO$_3$)O$_2$ at 600 °C, to Ce$_x$La$_{1-x}$(OH)$_3$ at 800 °C, final to (Ce$_x$La$_{1-x}$)$_2$O$_{3-\delta}$ at 900 °C were employed, while the original morphology was essentially unchanged. The dopant concentration was varied from 5 to 20 of cerium ions per LaCO$_3$OH nanoparticle. The X-ray diffraction (XRD) results reveal that the cerium dopant could enter easily into the LaCO$_3$OH structural lattice, whereas copper could unlikely enter into their lattice because of their large ionic radius difference. The cerium oxidation state was controlled by changing doping concentration. The X-ray photoelectron spectroscopy (XPS) results reveal that only one Ce^{3+} oxidation state is in the as-synthesized Ce$_x$La$_{1-x}$CO$_3$OH samples with cerium concentration ranging from 5 to 20 mol %, whereas both 3+ and 4+ ones coexisted in 20 mol % Ce:LaCO$_3$OH structure. Remarkable luminescence emission intensity enhancement of 1.5−9.0 times were observed for Ce$_x$La$_{1-x}$CO$_3$OH samples with cerium concentration ranging from 5 to 20 mol %, after doping with an undoped LaCO$_3$OH.

1. Introduction

Self-assembled doped oxide nanostructures with specific morphology have attracted considerable attention in both fundamental research and potential application in recent years.[1−4] Incorporating metal ions of appropriate elements into host lattices yields a homogeneous mixed oxide solid-solution with desirable properties because the electronic state of the dopant is confined to a small volume as a quantum confinement.[5] The interfacial interactions of the heterojunction nanocomposites originate from electron transfer across the nanometer contact at the interface of dopant atoms and particles.[6] This electron exchange interaction introduces crystalline defects from the presence of oxygen vacancies in the structural lattices, which is expected to significantly enhance the application performance.[7,8] Controlled doping of metal atoms/molecules into oxide structures can manipulate their electronic and optical properties because the number of active electrons is modified.[9] The controlled syntheses of mesoporous metal doped oxide nanocomposites with large surface area have drawn rapidly growing interest because of not only the additional dopant-dependent functional properties but also the in situ assembly of small particles as a building block into larger complex architectures.[10,11] The novel properties of assembled three-dimensional (3D) nanoarchitectures depend on the emergence of nanoscale properties as a result of the interparticle arrangement.[12] The realization of metal ion doped oxide nanoarchitectures with advanced functions thus requires the

*To whom correspondence should be addressed. E-mail: trong-on.do@gch.ulaval.ca.

(1) Talapin, D. V.; Shevchenko, E. V.; Bodnarchuk, M. I.; Ye, X.; Chen, J.; Murray, C. B. *Nature* **2009**, *461*, 964–967.
(2) Yang, Y.; Wang, C. *Chem. Soc. Rev.* **2009**, *38*, 2576–2589.
(3) Zhao, Y.; Jiang, L. *Adv. Mater.* **2009**, *21*, 1–18.
(4) Pileni, M. P. *Macromol. Symp.* **2008**, *270*, 14–26.
(5) Galli, G. *Nature* **2005**, *436*, 32–33.
(6) Erwin, S. C.; Zu, L.; Haftel, M. I.; Efros, A. L.; Kennedy, T. A.; Norris, D. J. *Nature* **2005**, *436*, 91–94.
(7) Yu, J. H.; Liu, X.; Kweon, K. E.; Joo, J.; Park, J.; Ko, K. T.; Lee, D. W.; Shen, S.; Tivakornsasithorn, K.; Son, J. S.; Park, J. H.; Kim, Y. W.; Hwang, G. S.; Dobrowolska, M.; Furdyna, J. K.; Hyeon, T. *Nat. Mater.* **2010**, *9*, 47–53.

(8) Ristein, J. *Science* **2006**, *313*, 1057–1058.
(9) Wang, F.; Han, Y.; Lim, C. S.; Lu, Y.; Wang, J.; Xu, J.; Chen, H.; Zhang, C.; Hong, M.; Liu, X. *Nature* **2010**, *463*, 1061–1065.
(10) Simon, J.; Protasenko, V.; Lian, C.; Xing, H.; Jena, D. *Science* **2010**, *327*, 60–64.
(11) Claridge, S. A.; Castleman, A. W.; Khanna, S. N.; Murray, C. B.; Sen, A.; Weiss, P. S. *ACS Nano* **2009**, *3*, 244–255.
(12) Lou, X. W.; Archer, L. A.; Yang, Z. *Adv. Mater.* **2008**, *20*, 3987–4019.

development of efficient synthetic approaches for the combination of the building blocks into complicated structures.

Because of the empty 4f shell of La^{3+} and the lack of electronic f-f transitions, cerium doped lanthanum(III) carbonate hydroxide ($Ce_xLa_{1-x}CO_3OH$) has drawn a great deal of interest as a promising luminescent material.[13,14] This advance is mainly due to their unique electronic and optical properties arising from the 4f electrons of cerium.[15] Cerium dopant incorporation is as a substitutial ion with compensating oxygen vacancies, which can be improved the reactive performance of $LaCO_3OH$ materials because of the generation of the crystalline defects.[16,17] These make cerium doped $LaCO_3OH$ materials to find various potential applications in catalysts,[18] high-quality phosphors,[19] up-conversion materials,[20] oxygen-ion conducting electrolytes.[21] Lanthanide carbonate hydroxide can be formed readily from the combination of lanthanide oxide with carbonate or carbonyl species in the presence of water or hydroxide.[22] Upon annealing at high temperature in the range of 600−900 °C, lanthanide carbonate hydroxides could be converted to their respective oxides by decarbonation and dehydration processes.[22] Considerable efforts have recently been devoted to preparing $LaCO_3OH$ micro/nanomaterials. For example, Fang et al.[23] synthesized the hexagonal-phase $LaCO_3OH$ microspheres from the hydrothermal reaction of $La(NO_3)_3 \cdot 6H_2O$ in the presence of $CO(NH_2)_2$. Popa et al.[24] reported the solvent-free synthesis of $LaCO_3OH$ superstructures from the thermal dissociation of the lanthanum acetate hydrate precursor under autogenic pressure at elevated temperature process. Han et al.[25] synthesized the $LaCO_3OH$ nanowires via a solvothermal process controlling the volume ratio of tetramethylguanidinium lactate to water solvent. Nevertheless, it is often difficult to bring cerium into the bulk interior of $LaCO_3OH$ nanoparticles by these methods. The cerium-doped lanthanum compound materials where cerium is often located on the surface or in the surface region or where at least the doping level is low. Thus, major limitations still emerge in advanced synthetic approaches for $Ce_xLa_{1-x}CO_3OH$ homogeneous structure and their mixed oxide derivative with large surface area, possibly because of the difficulty in choosing appropriate precursors and synthetic method. To obtain monodisperse and homogeneous $Ce_xLa_{1-x}CO_3OH$ nanocomposites, using binary cerium−lanthanum complex as precursor with similar decomposition temperature to generate stable mixed precursor

monomers in bulk solution is really required.[26] This can reduce the diffusion path of the spontaneous crystallization of cerium and lanthanum nuclei for the formation of the compositional and structural uniformity of $Ce_xLa_{1-x}CO_3OH$. One of the more successful protocols is a powerful two-phase method for synthesizing novel metal,[27] metal oxide,[28] semiconductor[29] nanoparticles. Very recently, we reported the general synthesis of rare earth oxide nanocrystals via thermolysis of the rare earth-oleate complex precursors in two-phase system containing *tert*-butylamine/oleylamine under autoclaving at 180 °C for 24 h.[30] This protocol allowed a variety of oxide nanocrystals to be synthesized in a toluene−water mixture using metal complexes as starting materials, which is inexpensive, uses low reaction temperature, and is easily obtained.

In the continuation of the development of a simple two-phase approach of synthesizing uniform-sized nanocrystals, herein, we report the fabrication of undoped and cerium doped $LaCO_3OH$ annular-shaped nanoarchitectures with large specific surface area via the thermolysis of the binary source precursor, $Ce_xLa_{1-x}(oleate)_3$ complex ($x = 0−20$ mol %), in a water−toluene system containing *tert*-butylamine/oleylamine. A possible growth mechanism for the self-assemblied $Ce_xLa_{1-x}CO_3OH$ annular-shaped nanoarchitectures is proposed. After annealing at 900 °C, the $Ce_xLa_{1-x}CO_3OH$ structure was easily converted to the derived mixed oxide particles, which kept their original morphology. The partial replacement of lanthanum by cerium ion and the surface composition and oxidation state of cerium dopant in the $LaCO_3OH$ structural lattice were confirmed by X-ray diffraction (XRD) and X-ray photoelectron spectroscopy (XPS) techniques. The luminescence emission intensity of the cerium-doped $LaCO_3OH$ samples was found to be enhanced as compared to that of undoped $LaCO_3OH$ sample.

2. Experimental Section

Starting Materials. All chemicals were used as received without further purification. Lanthanium(III) nitrate hexahydrate [$La(NO_3)_3 \cdot 6H_2O$, 99.9%], cerium(III) nitrate hexahydrate (Ce-$(NO_3)_3 \cdot 6H_2O$, 99.9%), copper(II) nitrate hexahydrate [$Cu(NO_3)_3 \cdot 6H_2O$, 98%], oleylamine ($C_{18}H_{35}NH_2$ or OM, technical grade, 70%), potassium oleate ($C_{18}H_{35}COOK$, 40% water), and *tert*-butylamine [$(CH_3)_3CNH_2$, 98%] were purchased from Sigma-Aldrich. All solvents used such as toluene and ethanol were of analytical grade and purchased from Reagent ACS.

Annular-Shaped $Ce_xLa_{1-x}CO_3OH$ ($x = 0−20$ mol %) Nanoarchitectures. The preparation of $Ce_xLa_{1-x}(oleate)_3$ complex (i) and the formation of nanoannular products (ii) consists of two steps.

(i). Preparation of $Ce_xLa_{1-x}(oleate)_3$ Complex. An organic solution was prepared by adding 160 mL of toluene into ethanol solution (80 mL) containing potassium oleate (21.31 g or 26.64 mmol). Subsequently, the organic phase was mixed with 80 mL of an aqueous solution of $Ce(NO_3)_3 \cdot 6H_2O$ (0−1.78 mmol) and $La(NO_3)_3 \cdot 6H_2O$ (8.88−7.10 mmol) with designed lanthanide molar ratios, and transferred to a flask. The stock two-phase mixture was heated to 70 °C for 6 h with vigorous stirring, and the organic solution turned light yellow after the reaction, indicating the occurrence of the coordinative reaction

(13) Koen, B. *Chem. Rev.* **2009**, *109*, 4283−4374.
(14) Bunzli, J. C. G. *Chem. Rev.* **2010**, *110*, 2729−2755.
(15) Su, L. T.; Tok, A. I. Y.; Zhao, Y.; Ng, N.; Boey, F. Y. C. *J. Phys. Chem. C* **2009**, *113*, 5974−5979.
(16) Meiser, F.; Cortez, C.; Caruso, F. *Angew. Chem., Int. Ed.* **2004**, *43*, 5954−5957.
(17) Ding, S. J.; Zhang, D. W.; Wang, P. F.; Wang, J. T. *Mater. Chem. Phys.* **2001**, *68*, 98−104.
(18) Sun, C. W.; Sun, J.; Xiao, G. L.; Zhang, H. R.; Qiu, X. P.; Li, H.; Chen, L. Q. *J. Phys. Chem. B* **2006**, *110*, 13445−13452.
(19) Mai, H. X.; Zhang, Y. W.; Si, R.; Yan, Z. G.; Sun, L. D.; You, L. P.; Yan, C. H. *J. Am. Chem. Soc.* **2006**, *128*, 6426−6436.
(20) Auzel, F. *Chem. Rev.* **2004**, *104*, 139−173.
(21) Etsell, T. H.; Flengas, S. N. *Chem. Rev.* **1970**, *70*, 339−376.
(22) Foger, K.; Hoang, M.; Turney, T. W. *J. Mater. Sci.* **1992**, *27*, 77−82.
(23) Zhang, Y.; Han, K.; Cheng, T.; Fang, Z. *Inorg. Chem.* **2007**, *46*, 4713−4717.
(24) Pol, V. G.; Thiyagarajan, P.; Moreno, J. M. C.; Popa, M. *Inorg. Chem.* **2009**, *48*, 6417−6424.
(25) Li, Z.; Zhang, J.; Du, J.; Gao, H.; Gao, Y.; Mu, T.; Han, B. *Mater. Lett.* **2005**, *59*, 963−965.
(26) Bao, N.; Shen, L.; Wang, Y.; Padhan, P.; Gupta, A. *J. Am. Chem. Soc.* **2007**, *129*, 12374−12375.

(27) Castro, E. G.; Salvatierra, R. V.; Schreiner, W. H.; Oliveira, M. M.; Zarbin, A. J. G. *Chem. Mater.* **2010**, *22*, 360−370.
(28) Nguyen, T. D.; Mrabet, D.; Do, T. O. *J. Phys. Chem. C* **2008**, *112*, 15226−15235.
(29) Pan, D.; Jiang, S.; An, L.; Jiang, B. *Adv. Mater.* **2004**, *16*, 982−985.
(30) Nguyen, T. D.; Do, T. O. *Phys. Chem. C* **2009**, *113*, 11204−11214.

Scheme 1. Two-Phase Protocol for the Synthesis of the Undoped and Cerium Doped $LaCO_3OH$ Annularshaped Nanoarchitectures
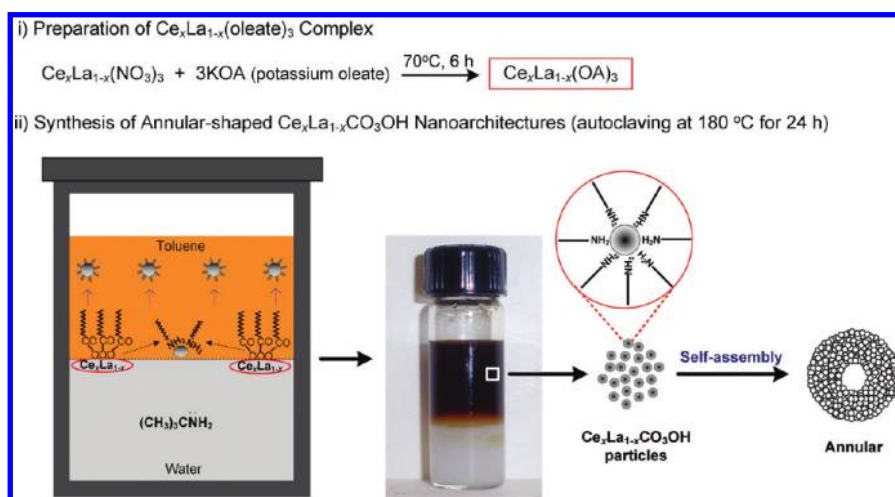
between binary metal (Ce^{3+}, La^{3+}) cations and oleate anions for the complex formation. The Ce^{3+}, La^{3+}/oleate molar ratio is close to 1:3, $Ce_xLa_{1-x}(oleate)_3$ with x of 0, 5, 10, 15, 20 mol %. The upper homogeneous toluene supernatant phase (160 mL) containing $Ce_xLa_{1-x}(oleate)_3$ complexes was washed several times with distilled water in a separatory funnel. After washing and drying in an oven at 80 °C for 24 h, the toluene and trace water was evaporated off, yielding the $Ce_xLa_{1-x}(oleate)_3$ complex in solid form. A 5.0 mol %$Cu,La(oleate)_3$ complex was obtained from a toluene/water–ethanol mixture containing 0.44 mmol $Cu(NO_3)_2 \cdot 6H_2O$, 8.43 mmol $La(NO_3)_3 \cdot 6H_2O$, 21.31 g of potassium oleate, in which the preparative procedure carried out under the same condition as that used to prepare $Ce_xLa_{1-x}(oleate)_3$ complex.

(ii). Synthesis of Annular-Shaped $Ce_xLa_{1-x}CO_3OH$ Nano-architectures. A 0.72 g portion of $Ce_xLa_{1-x}(oleate)_3$ complex solid (after toluene elimination) was dissolved in 20 mL of toluene solution under stirring at room temperature for 24 h. Five milliliters of oleylamine was added to the above homogenerous complex solution under stirring for 10 min. This organic solution was then transferred to a 70 mL Teflon-lined stainless steel autoclave containing an aqueous solution (20 mL) in the presence of *tert*-butylamine (0.15 mL). The autoclave was seated and heated to the crystallization temperature at 180 °C for 24 h. The colloidal nanoparticle products in the toluene phase were precipitated by adding excess of ethanol and recovered by centrifugation. This approach was extended to synthesize the copper-doped $LaCO_3OH$ heterogenerous nanoarchitectures. Typically, this sample was synthesized using 5.0 mol % $Cu,La(oleate)_3$ complexes under the same synthetic conditions of annular-shaped $Ce_xLa_{1-x}CO_3OH$ nanoarchitectures.

Characterization. XRD patterns were recorded on a Bruker SMART APEXII X-ray diffractometer, using Cu K_α radiation ($\lambda = 1.5418$ Å). Scanning electron microscope (SEM) images and elemental dispersive spectrum (EDS) analysis were obtained from a JEOL 6360 instrument working at 3 kV. Transmission electron microscope (TEM) images and selected area electron diffraction (SAED) patterns were obtained on a JEOL JEM 1230 operated at 120 kV. High-resolution TEM images and Fast Fourier transform (FFT) analysis were taken on a JEOL field-emission transmission electron microscope (2100F) operated at 200 kV. Samples were prepared by placing a drop of a dilute toluene dispersion of product onto a 200 mesh carbon coated copper grid and immediately evaporated at ambient temperature. XPS was carried out in an ion-pumped chamber (evacuated to 10^{-9} Torr) of a photoelectron spectrometer (Kratos Axis-Ultra) equipped with a focused X-ray source (Al$K\alpha$, $hv = 1486.6$ eV). The binding energy of the samples

was calibrated by setting the C 1 s peak to 285 eV. The peaks were deconvoluted by means of a standard CasaXPS software (v.2.3.13; product of CasaXPS Software Ltd., U.S.A.) to resolve the separate constituents after background subtraction. FTIR spectra were measured with FTS 45 infrared spectrophotometer with the KBr pellet technique. The specific area was calculated from the linear part of the Brunauer–Emmett–Teller equation ($P/P_o \approx 0.05-0.4$). The pore diameter distribution was obtained from analysis of the desorption branch of the isotherms using the Barrett–Joyner–Halenda model. The room temperature photoluminescence (PL) emission spectra were measured on an optical spectrum analyzer (ANDO AQ6317, Japan).

3. Results and Discussion

Two-phase synthesis of undoped and cerium doped La-CO_3OH ($Ce_xLa_{1-x}CO_3OH$, $x = 0-20$ mol %) homogeneous annular-shaped nanoarchitectures involves two steps, as shown in Scheme 1: (i) the preparation of $Ce_xLa_{1-x}(oleate)_3$ complex from the reaction between respective lanthanide nitrate and potassium oleate in a water–toluene mixture; (ii) the formation of mesoporous $Ce_xLa_{1-x}CO_3OH$ annular-shaped nanoarchitectures in an autoclave containing a water–toluene mixture composed of $Ce_xLa_{1-x}(oleate)_3$/*tert*-butyl-amine/oleylamine at 180 °C for 24 h. According to the classical LaMer diagram,[31] the formation process of the colloidal $Ce_xLa_{1-x}CO_3OH$ nanoarchitectures can be well understood by the reported two-stage growth model, in which nanosized crystalline precursors are nucleated first in supersaturated solution at the water–toluene interface and then the initially formed seeds aggregate into a larger secondary nanoarchitecture. The $Ce_xLa_{1-x}CO_3OH$ nanoarchitectures were capped by the amine groups of oleylamine molecules, the exposed hydrophobic alkyl groups were well-immersed in toluene, and guaranteed the good dispersibility of the product in the toluene phase. No product was observed in the water phase. The solid-solution cerium–lanthanum oxide particles were produced from the decarbonation and dehydration of $Ce_xLa_{1-x}CO_3OH$ upon annealing.

Undoped lanthanum-compound sample synthesized using $La(oleate)_3$ complex. The formation of lanthanide oleate complex was illustrated by FTIR spectrum (in the Supporting Information, S-Figure 1). The XRD pattern (Figure 1a)

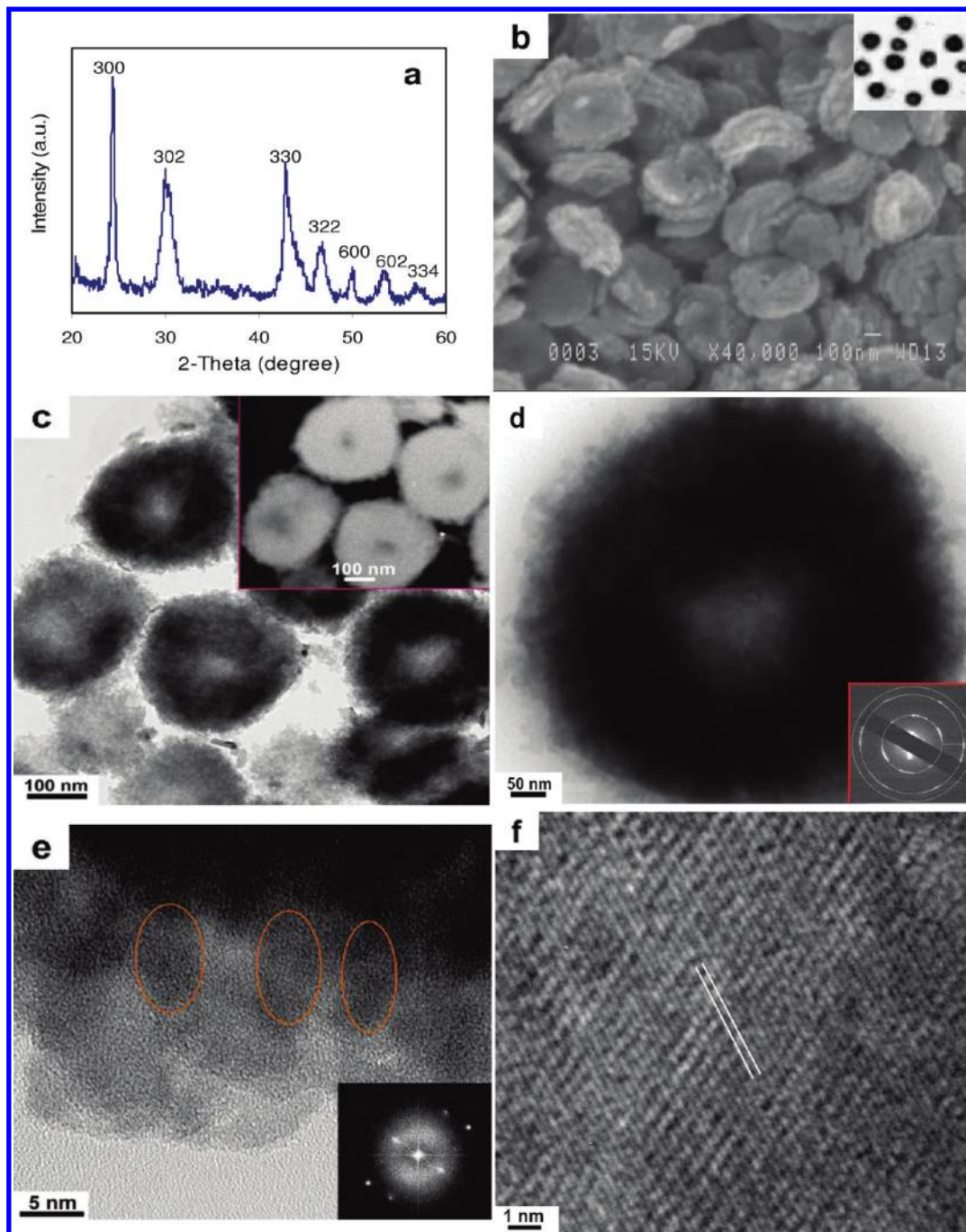(31) Meldrum, F. C.; Colfen, H. *Chem. Rev.* **2008**, *108*, 4332–4432.

Figure 1. (a) XRD; (b) SEM; (c) and (d) TEM, inset dark-field TEM, inset SAED; (e) and (f) HRTEM, inset FFT pattern of the as-synthesized $LaCO_3OH$ annular-shaped nanoarchitectures.

of the formed product without cerium dopant reveals that all diffraction peaks were perfectly indexed to a pure hexagonal-phase $LaCO_3OH$ structure with cell constants of $a = 5.22$ Å, $b = 5.22$ Å, $c = 11.42$ Å, which is consistent with a reference pattern JCPDS No. 05-0602.[32] No $La(OH)_3$ or La_2O_3 was found. The strong and sharp diffraction peaks demonstrate high crystallinity of the products. The broadening of the peaks confirms the nanoscale nature of the $LaCO_3OH$ structure. The average particle size was assessed from the (302) peak at $2\theta = 30.2°$ using the Scherrer equation, revealing that the

resulting product consists of the small particles of $\sim 3-5$ nm in size. This indicates that the $LaCO_3OH$ nanostructures are composed of numerous small particle assemblies. The SEM image in Figure 1b shows that a uniform population of $LaCO_3OH$ nanostructures with an interesting annular shape each containing an interior concavity in the sphere were observed. The monodisperse annular-shaped nanoarchitectures presented a rough surface, narrow size distribution, and an average particle diameter of ~ 400 nm. TEM images in Figure 1c indicate that the distribution of small particles at the center of each big $LaCO_3OH$ annular-shaped nanoarchitecture is less than that of their edges, confirming the annular structure. Dark-field TEM image (Figure 1d) of this sample

(32) Joint Committee on Powder Diffraction Standards diffraction data file no. 13–434; International Center for Diffraction Data: Newtown Square, PA, U.S.A., 1963.
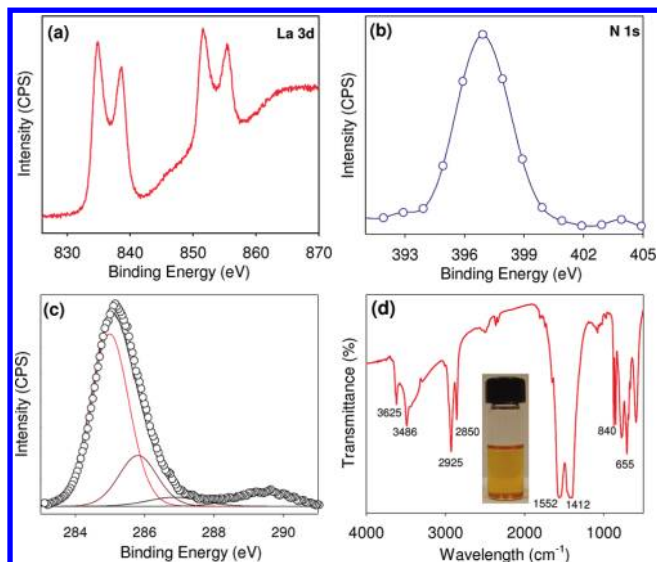
Figure 2. (a) La 3d; (b) N 1s; (c) C 1s XPS; (d) FTIR spectra of the as-synthesized $LaCO_3OH$ nanoannulars; Inset of (d): one photo of transparent toluene solution containing the colloidal $LaCO_3OH$ nanoannulars.

Figure 3. Nitrogen adsorption−desorption and pore size distribution of the as-made $LaCO_3OH$ nanoannulars after annealing at 550 °C for 2 h. Inset SEM image of the calcined $LaCO_3OH$ annular sample.

shows a clear contrast between ring and interior concavity, confirming the doughnut structure. Figure 1d shows a single $LaCO_3OH$ annular-shaped nanoarchitecture with a diameter of ~400 nm. From the HRTEM image shown in Figure 1e,f, the lattice space of a single particle was clearly observed, and it further displays that the annular nanoarchitecture is composed of numerous small interconnected primary nanoparticles with a size of 3−5 nm, in good agreement with the XRD result. The SAED pattern (inset of Figure 1d) confirms the polycrystalline nature of the self-assembled annular nanoarchitectures. Fast Fourier Transform (FFT) analysis (inset of Figure 1e) shows the crystallographic nature of the small particle assembly.

Oleylamine-capped $LaCO_3OH$ annular-shaped nanoarchitectures were characterized by the XPS technique for the evaluation of the surface composition, oxidation state, and capping oleylamine on the particle surface (Figure 2). Survey XPS spectrum and elemental dispersive spectrum (EDS) analysis detected the presence of La, C, O elements (S-Figure 2). La 3d XPS spectrum (Figure 2a) shows that the La $3d_{5/2}$ peaks center at ~640.59−652.01 eV, and La $3d_{3/2}$ peaks center at ~642.20−653.60 eV, with $\Delta \approx 1.6$ eV, corresponding to La^{3+}, which is consistent with those of bulk La_2O_3 phase.[33] The splitting (Δ) is due to spin orbit interaction and charge transfer from O 2p to La 4f. The N 1s region (Figure 2b) contained a single peak at 399.8 eV, assigned to nitrogen in the -NH_2 group of the oleylamine molecule. The C 1s spectrum (Figure 2c) exhibits that the peaks at 284.6, 288.3, 288.3 eV were attributed to alkyl chain, C−N, carbonate, respectively, indicating that the $LaCO_3OH$ nanoarchitectures were covered with the oleylamine molecules.[34] FTIR spectrum of oleylamine-capped $LaCO_3OH$ nanoarchitectures is shown in Figure 2d. The shape absorption peaks at 3625 and 3468 cm^{-1} are assigned to the stretching vibration
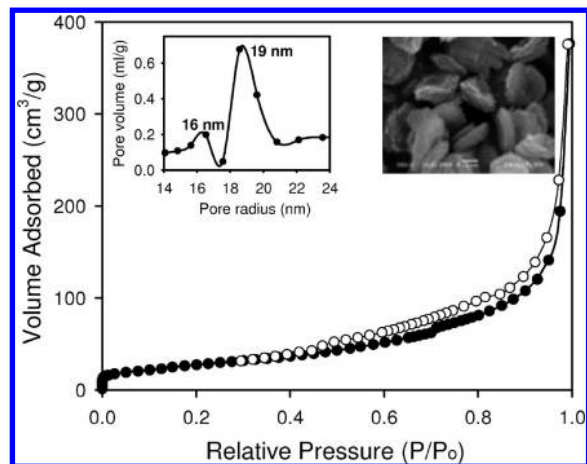
of structural OH and adsorbed H_2O, respectively.[35] The peaks at 2850−2925 cm^{-1} are attributed to the C−H stretching mode of alkyl chains of oleylamine molecules.[30] The strong peak at 1412 cm^{-1} is assigned to the stretching vibration of the -NH_2 group of oleylamine.[30] Four modes of the CO_3^{2-} ion of $LaCO_3OH$ appeared at 1070−1100 cm^{-1} (ν_1), 850−880 cm^{-1} (ν_2), 1400 cm^{-1} (ν_3), and 690−730 cm^{-1} (ν_4).[35] Moreover, one photograph of the transparent toluene solution containing colloidal $LaCO_3OH$ nanoarchitectures is shown in the inset Figure 2d. These data further confirm that the -NH_2 groups of oleylamine molecules are capped on the particle surface. The exposed hydrophobic alkyl groups were oriented outward, and thus the capped products were highly dispersed in toluene.

The oleylamine is fully decomposed when the $LaCO_3OH$ nanoarchitectures are thermally treated at 550 °C for 2 h. The thermal-stabilized nanoarchitectures therefore become mesoporous, as shown in the SEM image (inset of Figure 3). Figure 3 shows that the calcined $LaCO_3OH$ sample reveals a typical type-IV isotherm with H1-type hysteresis, characteristic of mesoporous materials,[36] with Brunauer−Emmett−Teller (BET) surface area of ~100 m^{2}g^{-1}. The high surface area of the calcined self-assembled nanoannulars could be due to the individual surface area of 3−5 nm $LaCO_3OH$ particles after calcination. The pore size distribution obtained using the Barrett−Joyner−Halenda (BJH) method (inset of Figure 3) shows the bimodal pore distributions at 20 and 16 nm. This could be due to the porosity of interparticles, which is consistent with the results of SEM/TEM observations. The void structure is expected to arise from the self-assembly of 3−5 nm particles. Large external pores were generated by the formation of a large concavity in the center of annular-shaped structures, while small internal pores were formed the interstitial voids inside the annular-shaped $LaCO_3OH$ nanoarchitectures. Obviously, such novel mesoporous $LaCO_3OH$ nanoarchitectures with high surface area and rough surface can be useful for the catalytic performance.

Because of the La(oleate)$_3$ complex solid (after toluene elimination) having high thermal stability, the thermolysis rate of these complexes at the water−toluene interface is relatively slow. The oleylamine-capped seeds with small in size were produced. These formed small seeds are active because

(33) Moulder, J. F.; Stickle, W. F.; Sobol, P. E.; Bomben, K. D. *Handbook of X-ray photoelectron spectroscopy*; Perkin-Elmer corporation, Physical Electronics Division: Minneapolis, MN, 1992.

(34) Deng, Z.; Peng, B.; Chen, D.; Tang, F.; Muscat, A. J. *Langmuir* **2008**, *24*, 11089–11095.

(35) Sun, J.; Kyotani, T.; Tomita, A. *J. Solid State Chem.* **1986**, *65*, 94–99.

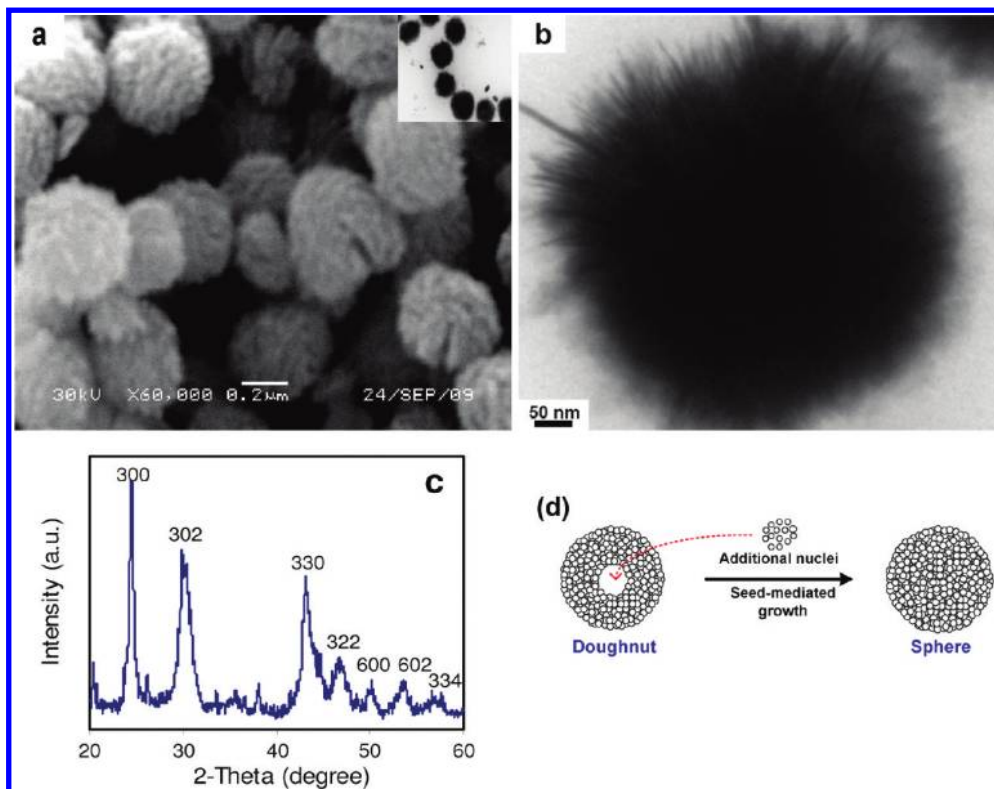(36) Li, Y.; Cao, M.; Feng, L. *Langmuir* **2009**, *25*, 1705–1712.

Figure 4. (a) SEM; (b) TEM; (c) XRD pattern of the as-synthesized LaCO$_3$OH nanospheres; (d) a schematic model of the shape change from annular into sphere by the seed-mediated growth.

of their high surface energy and tend to aggregate growth, leading to the formation of larger aggregates to minimize the interface energy. A possible formation mechanism of the LaCO$_3$OH structure using La(oleate)$_3$ complex, *tert*-butylamine, and capping oleylamine, is depicted in eq 1. The formation of LaCO$_3$OH structure could consist of three steps during the solvo-hydrothermal synthesis: (i) *tert*-butylamine as nucleophile attacks one carboxyl group of the oleate ligand through a S$_N^1$ mechanism, in which a lone pair of electrons of the donor NH$_2$ group shares with the electrophilic carboxyl center at the nucleation stage. *Tert*-butylamine can react with the oleate group but not with oleylamine because its basic property is stronger than that of oleylamine. Moreover, *tert*-butylamine is dispersed an aqueous phase and easily hydrolyzed to generate OH$^-$ compared with oleylamine in organic phase. (ii) This nucleophilic reaction leads to C–O bond cleavage and the release of lanthanum-oxyl and carbonyl species. (iii) The LaCO$_3$OH structure was formed from the combinative reaction of lanthanum-oxyl, carbonyl, and hydroxyl species at the water–toluene interface.
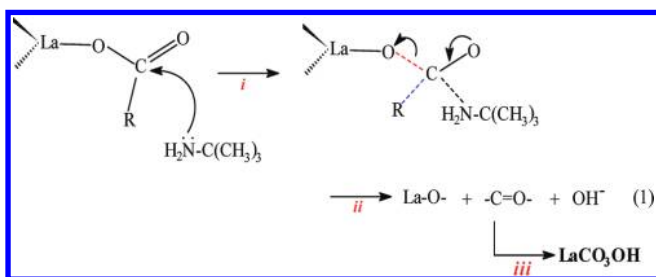
The seed-mediated growth has recently been employed for the synthesis of larger metallic nanoparticles on smaller seeds, meaning that the growth process is separated from additional

nucleation.[37] For example, Hyeon and co-workers[38] synthesized the monodisperse iron oxide nanoparticles with continuous size spectrum of 6–13 nm from the combination of various-sized iron oxide nanoparticles and the iron-oleate complex solution via thermal decomposition. In this work, a similar principle is expected to apply for the synthesis of colloidal LaCO$_3$OH nanospheres by the additional incremental growth. The annular-shaped LaCO$_3$OH nanoarchitecture as seed and La(oleate)$_3$ complex as additional growth source were used. Twenty milligrams of presynthesized 400 nm LaCO$_3$OH annular-shaped nanoarchitectures was dispersible to 10 mL of toluene under stirring, and then added to a water–toluene (20:10 mL) mixture containing 0.24 g of La(oleate)$_3$ and 0.05 mL of *tert*-butylamine. Under autoclaving at 180 °C for 10 h, La(oleate)$_3$ complexes were decomposed to produce LaCO$_3$OH nuclei under catalyzing *tert*-butylamine. These nuclei directly grow on the surface of LaCO$_3$OH doughnut seeds by a digestive ripening mechanism leading to the formation of final annular-shaped LaCO$_3$OH nanoarchitectures. SEM image (Figure 4a) depicts that the morphology of the product has a spherical shape with the diameter unchanged (∼400 nm), but any voids at the center of each sphere were not observed. The TEM image (Figure 4b) indicates that the self-assembled nanospheres without void consist of small particles. The XRD pattern (Figure 4c) of the as-synthesized LaCO$_3$OH nanospheres also exhibits a pure hexagonal structure, and the intense and broadening diffraction peaks are significantly unchanged. A schematic drawing of the shape change from annular-shaped

(37) Chen, A.; Hindle, P. H. *Chem. Rev.* **2010**, *110*, 3767–3804.
(38) Park, J.; Lee, E.; Hwang, N. M.; Kang, M.; Kim, S. C.; Hwang, Y.; Park, J. G.; Noh, H. J.; Kim, J. Y.; Park, J. H.; Hyeon, T. *Angew. Chem.* **2005**, *117*, 2932–2937.
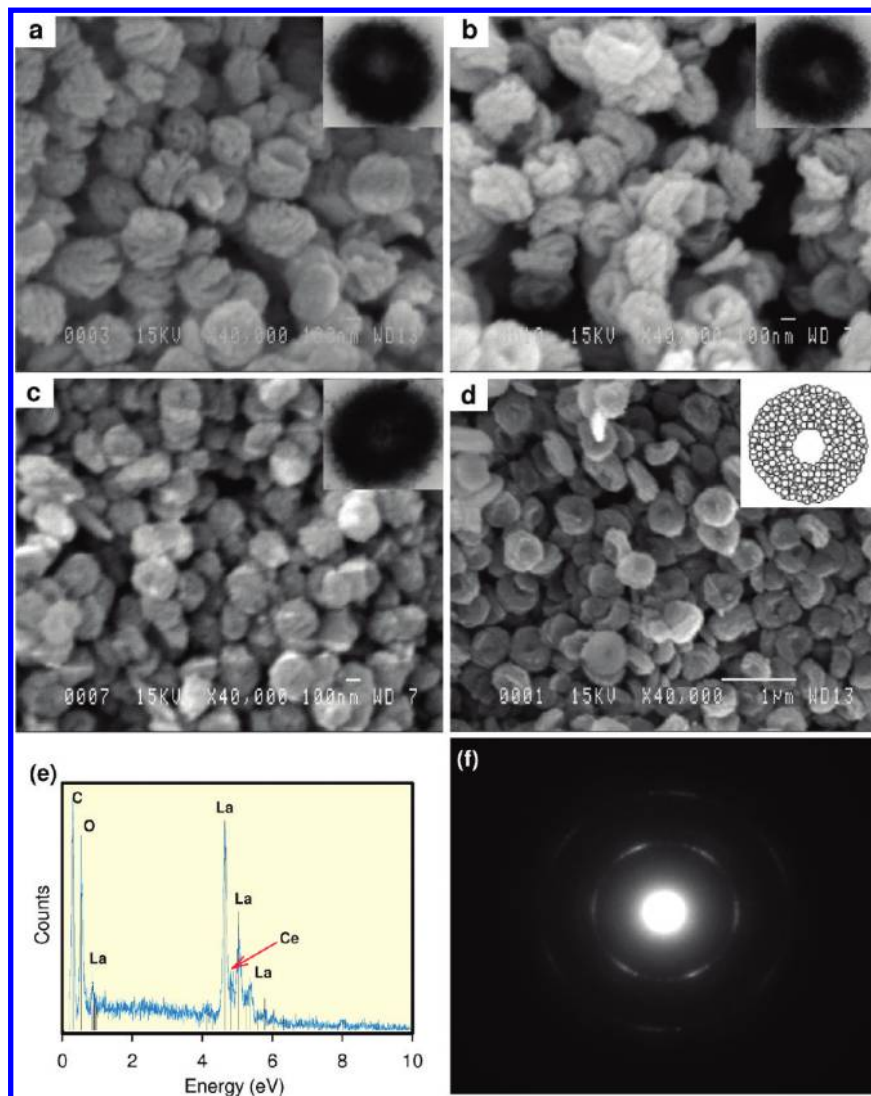
Figure 5. SEM images of the $Ce_xLa_{1-x}CO_3OH$ nanoannulars with various doping level (mol %): (a) $x = 5$; (b) $x = 10$; (c) $x = 15$; (d) $x = 20$; (e) EDS and (f) SAED pattern of 15 mol % cerium doped sample. The upper insets in (a–c) show the TEM images of a corresponding annular-shaped nanoarchitecture. The upper inset in (d) showing a drawn scheme of an annular structure.

architecture into a sphere by the seed-mediated growth is illustrated in Figure 4d.

$LaCO_3OH$ compound can be doped with various lanthanide elements to form a nanostructured mixed oxides. Exploiting this sensitivity can allow their physical and chemical properties to be controlled with atomic-scale precision, and can result in materials tailored to possess specific properties. In this second work, the cerium doped $LaCO_3OH$ samples with cerium dopant concentration of 5, 10, 15, 20 mol % using binary complex precursor, $Ce_x,La_{1-x}(oleate)_3$ with x of 5, 10, 15, 20 mol %, respectively. SEM images in Figure 5 show that the particle size and shape of all the Ce_xLa_{1-x}-CO_3OH samples with various doping levels (5–20 mol %) are similar to those of undoped $LaCO_3OH$ annular-shaped nanoarchitectures. The 400 nm-sized $Ce_xLa_{1-x}CO_3OH$ annular-shaped nanoarchitectures with various doping levels were made up of many particles and were polycrystalline in nature as indicated by the inset TEM and SAED results (inset of Figure 5a–f). Corresponding to the elemental dispersive spectrum (EDS) analysis (Figure 5e) of the representative 15 mol % cerium doped $LaCO_3OH$ sample reveals the molar ratio of Ce and La content is similar with the original ratio of

reagents. The morphology of the doped products did not substantially vary when an increase in the amount of further doping, suggesting that cerium ions tend to solubilize into the $LaCO_3OH$ lattice leading to a homogeneous $Ce_xLa_{1-x}CO_3OH$ structure. The segregation of cerium ions on the surface of the annular-shaped nanoarchitecture seems to be limited.

Figure 6(a–d) displays XRD patterns of the as-synthesized cerium doped $LaCO_3OH$ annular-shaped nanoarchitecture samples with doping levels of 5, 10, 15, 20 mol %. The introduction of cerium seems not to modify the crystalline structure of pure $LaCO_3OH$. Indeed, cerium doped $LaCO_3OH$ still presents the hexagonal phase for all doping concentrations. All the doped samples show that no additional diffraction peaks corresponding to either cerium oxide or cerium hydroxide were detected at the current doping levels. This indicates that the cerium ions are completely dissolved in the $LaCO_3OH$ host lattice by substitution for lanthanum ions to yield a homogeneous $Ce_xLa_{1-x}CO_3OH$ structure. The calculation of the average particle sizes of four doped samples using the (302) peak at $2\theta = 30.2°$ also suggest that the $Ce_xLa_{1-x}CO_3OH$ nanoarchitectures are composed of the small particles of 3–5 nm in size. It is known that La ion

can exist in only one oxidation state of 3+ having an ionic radius of 1.172 Å, whereas Ce can exist in the 3+ (1.143 Å) and 4+ (0.97 Å) oxidation states. Only the Ce^{3+} oxidation state in the as-synthesized 5−15 mol % Ce:LaCO₃OH samples was observed, while both Ce^{3+} (38%) and Ce^{4+} (62%) oxidation states in 20 mol % Ce:LaCO₃OH were found (see the XPS results below). It was noted that for the 5−15 mol % Ce^{3+}:LaCO₃OH samples (in the absence of Ce^{4+}), no significant shift of the XRD peak positions was observed, consequently, no significant change in the lattice parameters of the doped samples, as compared to those of the undoped LaCO₃OH sample was observed (Figure 6a−c). This can be attributed to negligible difference in ionic radii of Ce^{3+} (1.150 Å) and La^{3+} (1.172 Å). However, for the 20 mol % cerium doped LaCO₃OH sample, with the presence of Ce^{4+}, the (302) peak was shifted lightly toward higher angle side owing to the partial substitution of Ce^{4+} with La^{3+} in the La-CO₃OH lattice (Figure 6d). We reasoned that the ionic radius

of Ce^{4+} (0.97 Å) is smaller than that of La^{3+} (1.172 Å), leading to a contraction in the unit-cell volume.

TGA-DTA curves (Supporting Information, S-Figure 3) were recorded for oleylamine (OM)-capped $Ce_xLa_{1-x}CO_3OH$ annular-shaped nanoarchitectures. The TGA curve shows that the total weight loss of the OM-capped $Ce_xLa_{1-x}CO_3$-OH sample is ∼46%, which is attributed to the combustion/elimination of oleylamine and the decarbonation of the conversion of $Ce_xLa_{1-x}CO_3OH$ to $Ce_xLa_{1-x}(OH)_3$ and finally to $(Ce_xLa_{1-x})_2O_{3-\delta}$. An intense exothermic peak at 351 °C in the DTA profile is attributed to the combustion and elimination of oleylamine. The weight loss because of the decarbonation of $Ce_xLa_{1-x}CO_3OH$ into $(Ce_xLa_{1-x})_2O_{3-\delta}$ is ∼7%, corresponding to weak exothermic DTA peaks at higher temperature (∼680−830 °C). A representative as-synthesized 10 mol % cerium doped LaCO₃OH annular sample was heat-treated at 300, 600, 800, 900 °C for 12 h in air to investigate the thermal stability and induce the formation of derived mixed oxide solid-solution. The thermal decomposition of $Ce_xLa_{1-x}CO_3OH$ structure at different calcined temperatures could be expressed in eqs 2, 3, and 4.

$$2Ce_xLa_{1-x}CO_3OH \xrightarrow{600\ °C} (Ce_xLa_{1-x})_2(CO_3)O_2 + CO_2 + H_2O \tag{2}$$

$$(Ce_xLa_{1-x})_2(CO_3)O_2 + 3H_2O \xrightarrow{800\ °C} 2Ce_xLa_{1-x}(OH)_3 + CO_2 \tag{3}$$

$$2Ce_xLa_{1-x}(OH)_3 \xrightarrow{900\ °C} (Ce_xLa_{1-x})_2O_{3-\delta} + 3H_2O \tag{4}$$

From evidence of the SEM images (Figure 7A), the samples annealed at 300, 600, 800 °C, show quite similar morphology to the untreated sample, indicating that the annular shape has a high thermal stability. When treated at 900 °C, the annular-shaped nanoarchitectures become smooth, and the agglomeration between both annulars appears because of the effect of sintering. Figure 7B shows XRD patterns of the
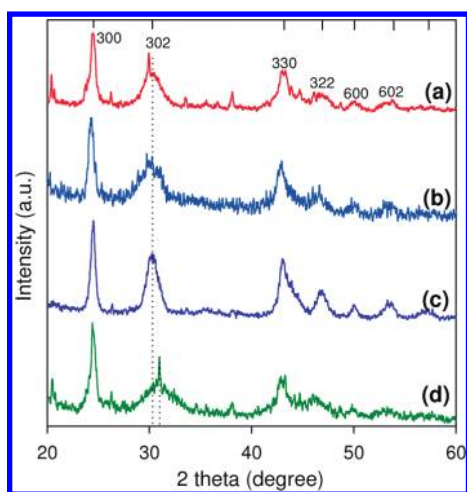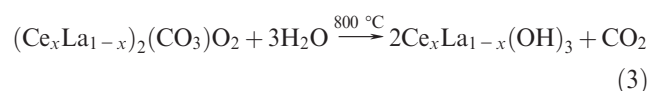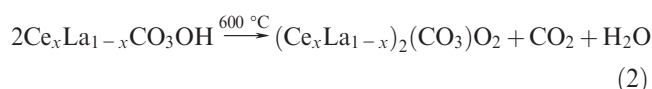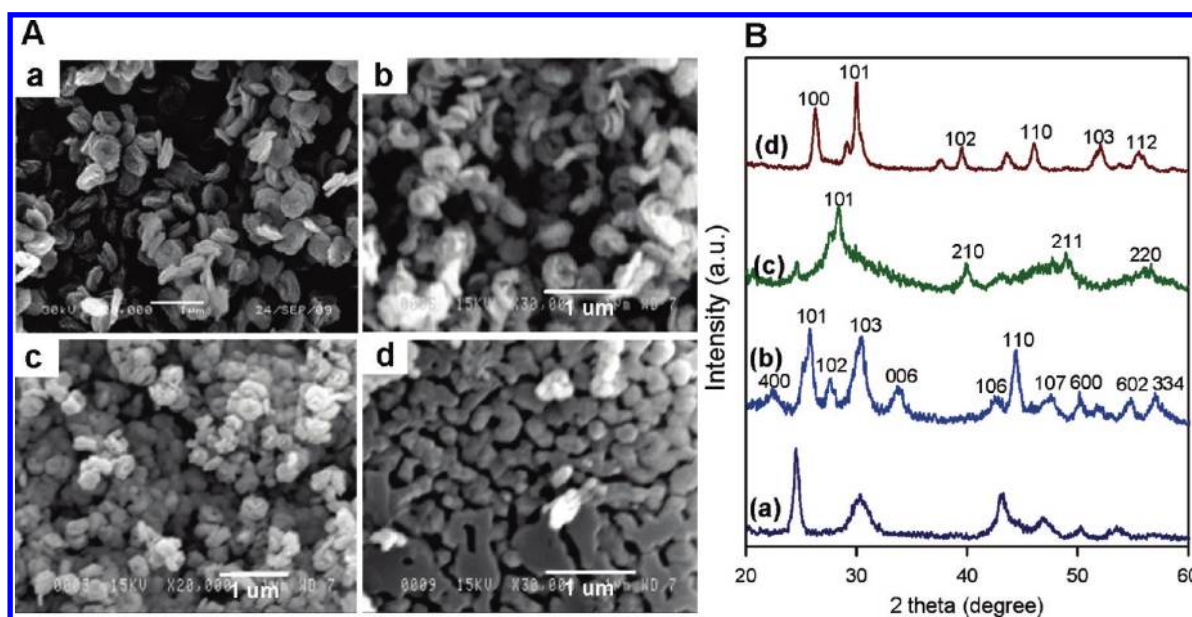

Figure 6. XRD patterns of the as-synthesized $Ce_xLa_{1-x}CO_3OH$ nano-annular samples with various doping levels (mol %): (a) $x = 5$; (b) $x = 10$; (c) $x = 15$; (d) $x = 20$.

Figure 7. (A) SEM images and (B) XRD patterns of the as-synthesized 10 mol % cerium doped LaCO₃OH samples calcined at the different temperatures for 12 h: (a) $Ce_xLa_{1-x}CO_3OH$, 300 °C; (b) $Ce_xLa_{1-x}(CO_3)O_2$, 600 °C; (c) $Ce_xLa_{1-x}(OH)_3$, 800 °C; (d) $(Ce_xLa_{1-x})_2O_{3-\delta}$, 900 °C.
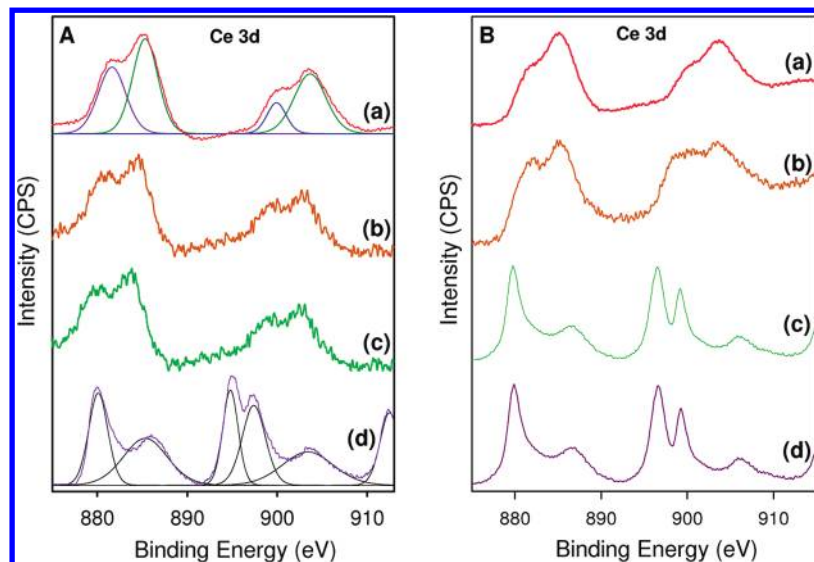
Figure 8. (A) Ce 3d XPS spectra of the as-synthesized $Ce_xLa_{1-x}CO_3OH$ samples with various doping levels (mol %): (a) $x = 5$; (b) $x = 10$; (c) $x = 15$; (d) $x = 20$. (B) Ce 3d XPS spectra of 10 mol % cerium doped $LaCO_3OH$ samples calcined at different temperatures for 12 h: (a) 300 °C; (b) 600 °C; (c) 800 °C; (d) 900 °C.

$Ce_xLa_{1-x}CO_3OH$ nanoarchitectures calcined at 300, 600, 800, 900 °C, which evidence the conversion of composition. The doped sample calcined at 300 °C still remains the hexagonal $Ce_xLa_{1-x}CO_3OH$ phase. This structure was converted into an hexagonal $(Ce_xLa_{1-x})_2(CO_3)O_2$ intermediate at 600 °C and into hexagonal $Ce_xLa_{1-x}(OH)_3$ at 800 °C by decarbonation. At 900 °C, $Ce_xLa_{1-x}(OH)_3$ was converted into hexagonal $(Ce_xLa_{1-x})_2O_{3-\delta}$ by the dehydration process. The width of diffraction peaks in the XRD patterns of the samples treated at 300, 600, 800 °C has no difference in particle size, suggesting that the small particle ($\sim$3−5 nm) in these samples still remained. However, as the treatment temperature was raised to 900 °C, the mean nanoparticle size is increased to 8.5 nm, confirming further the agglomeration of particles by heating.

The surface composition, the oxidation state, and the binding energy change of the cerium element in the doped $LaCO_3OH$ samples were identified by XPS. The N 1s and C 1s XPS (Supporting Information, S-Figure 4b,c) and FTIR (Supporting Information, S-Figure 4d) data of these doped samples also reveal their particle surface was capped by -NH_2 groups of oleylamine molecules. The La 3d XPS spectrum (Supporting Information, S-Figure 4a) of the doped sample is similar to that of the undoped $LaCO_3OH$ nanoarchitectures. As can be noted, with increase of dopant concentration, there is no change in the position and intensity of the La 3d core level peaks. Survey XPS results of these doped samples determined no other contaminants are detected, except for the above-mentioned elements. The Ce-to-La molar ratio of 5 mol % $Ce:LaCO_3OH$, 10 mol % $Ce:LaCO_3OH$, 15 mol % $Ce:LaCO_3OH$, 20 mol % $Ce:LaCO_3OH$ samples was spectrally estimated to be 4.5:96.5, 8.7:91.3, 13.1:86.9, 19.2:80.8, respectively, corresponding to $Ce_{0.045}La_{0.965}CO_3OH$, $Ce_{0.087}La_{0.913}CO_3OH$, $Ce_{0.131}La_{0.869}CO_3OH$, $Ce_{0.192}La_{0.808}CO_3OH$ formulas. The detected cerium concentrations were slightly lower than the initial starting concentrations of Ce_xLa_{1-x}-(oleate)$_3$ complexes, indicating the atomic mixing nature of the cerium and lanthanum ion sites.

Ce 3d XPS spectra (Figure 8Aa−c) of the as-synthesized samples of 5 mol % $Ce:LaCO_3OH$, 10 mol % $Ce:LaCO_3OH$,

and 15 mol % $Ce:LaCO_3OH$ exhibit Ce $3d_{5/2,3/2}$ peaks at 885.7−904.0 eV which are attributed to Ce^{3+}.[33] No peak was observed in the binding energy region of Ce^{4+}. However, the Ce $3d_{5/2,3/2}$ XPS spectrum (Figure 8Ad) of the as-synthesized 20 mol % $Ce:LaCO_3OH$ sample displays that cerium is in mixed valence states of 3+ (880.40, 885.5, 898.81, 903.7 eV) and 4+ (882.7, 888.96, 898.2, 901.3, 907, 916.7 eV).[33] On the basis of the peak areas, we found the surface concentration of Ce^{3+} and Ce^{4+} to be $\sim$38 and 62%, respectively. These results evidence the presence of Ce in predominantly 3+ oxidation state in the $Ce_xLa_{1-x}CO_3OH$ samples with dopant concentration ranging from 5 to 15 mol %. Both 3+ and 4+ oxidation states coexist in 20 mol % $Ce:LaCO_3OH$, in which a part of Ce^{3+} ions would be converted into Ce^{4+} during synthesis process. It is particularly noted that the Ce 3d peaks showed the shift by $\sim$0.8−1.0 eV toward lower binding energy with increasing dopant concentration. The decrease in binding energy can be attributed to an increase in valence electron density and the formation of Ce−La bonding structure.[39]

It was predicted that the oxidation state change of cerium dopant in the lanthanide compound is often related to crystalline defects and generated oxygen vacancy concentration, which would greatly influence the chemical properties.[40] Figure 8B shows the modifications of cerium oxidation states of a representative 10 mol % $Ce:LaCO_3OH$ sample, calcined at 300, 600, 800, 900 °C for 12 h. From the analysis of the XPS spectra, cerium ion in the samples calcined at 300 and 600 °C still exist in one oxidation state of 3+ (Figure 8Ba,b), whereas two cerium oxidation states (Ce^{3+} and Ce^{4+}) coexist in the samples calcined at 800 and 900 °C (Figure 8Bc,d). The Ce^{4+} concentration in the doped sample calcined 800 °C was found to be $\sim$41.2%, which increased to $\sim$75.5% upon annealing at 900 °C. The partial conversion of Ce^{3+} ion to Ce^{4+} took place on their surface upon annealing because of the oxidation of Ce^{3+} in air atmosphere. The difference of O 1s XPS spectra of

(39) Ahmad, A.; Shah, J. A.; Buzby, S.; Shah, S. I. *Eur. J. Inorg. Chem.* **2008**, 948–953.
(40) Luque, M. P. R.; Hernandez, J. C.; Yeste, M. P.; Bernal, S.; Cauqui, M. A.; Pintado, J. M.; Omil, J. A. P.; Stephan, O.; Calvino, J. J.; Trasobares, S. *J. Phys. Chem. C* **2008**, *112*, 5900–5910.
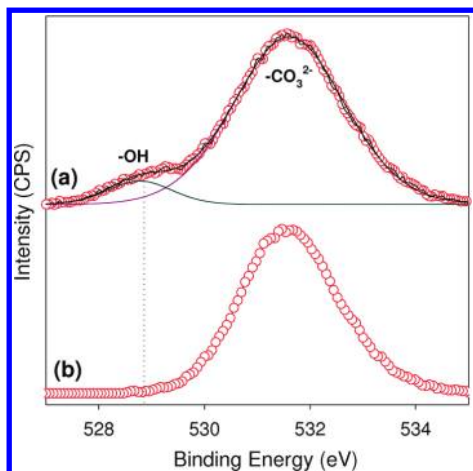
Figure 9. O 1s XPS spectra of (a) $Ce_xLa_{1-x}CO_3OH$ and (b) $(Ce_xLa_{1-x})_2O_{3-\delta}$ samples.

Figure 10. Photoluminescence emission spectra (under excitation at 360 nm) of the as-synthesized $Ce_xLa_{1-x}CO_3OH$ nanoannular samples with various doping levels (mol %): (a) $x = 0$; (b) $x = 5$; (c) $x = 10$; (d) $x = 15$; (e) $x = 20$. Inset: one photo of transparent toluene solution containing colloidal 10 mol % cerium doped $LaCO_3OH$ nanoannulars and the relationship between the cerium concentration and the PL intensity ratio.

the $Ce_xLa_{1-x}CO_3OH$ and $(Ce_xLa_{1-x})_2O_{3-\delta}$ samples were also observed (Figure 9). The $Ce_xLa_{1-x}CO_3OH$ sample is composed of two oxygen components, whereas the $(Ce_xLa_{1-x})_2O_{3-\delta}$ sample exhibits only one oxygen component. For the $Ce_xLa_{1-x}CO_3OH$ sample, the weak XPS peak at 529.4 eV is assigned to the hydroxide group, and the intense second one at 531.8 eV is attributed to the carbonate group. The $(Ce_xLa_{1-x})_2O_{3-\delta}$ sample exhibits only one O 1s XPS peak at 531.8 eV related to O—La,Ce bonds. This also indicates a high OH concentration on the particle surface of the $Ce_xLa_{1-x}CO_3OH$ sample.

To understand the effect of the cerium dopant concentration on the upconversion emission, photoluminescence (PL) emission spectra (Figure 10) of the colloidal $Ce_xLa_{1-x}CO_3OH$ nanoarchitectures with various doping levels ($x = 0-20$ mol %) in toluene were recorded on exciting at 360 nm. Using the same particle concentrations, the colloidal solutions of these $Ce_xLa_{1-x}CO_3OH$ samples show the same spectral peak positions at 424, 448, 486, 529, 560 nm, which can be attributed to the charge-transfer transition in the $Ce_xLa_{1-x}CO_3OH$ structure.[41,42] The broad backgrounds of the luminescence spectra of these doped samples can be due to the self-assembly of small nanoparticles (3−5 nm) for the formation of the aggregated $Ce_xLa_{1-x}CO_3OH$ structure with annular shape.[43] However, the observed effect of variation in emission can be correlated to the dopant concentration. Namely, the intensity was found to increase with increase in dopant concentration. We obtained the PL intensity enhancement of 1.5, 2.2, 5.0, 9.0 times for $Ce_xLa_{1-x}CO_3OH$ with doping level of 5, 10, 15, 20 mol %, respectively, after doping with an undoped $LaCO_3OH$. The emission intensity of $Ce_xLa_{1-x}CO_3OH$ sample increases with increase in cerium concentration to 20 mol % and then exhibits a gradual decrease upon further increase in cerium dopant content. The relationship between the cerium dopant concentration in $LaCO_3OH$ sample and the PL intensity ratio was shown in inset of Figure 10. The initial increase in emission intensity can be associated with the increase in relative concentration
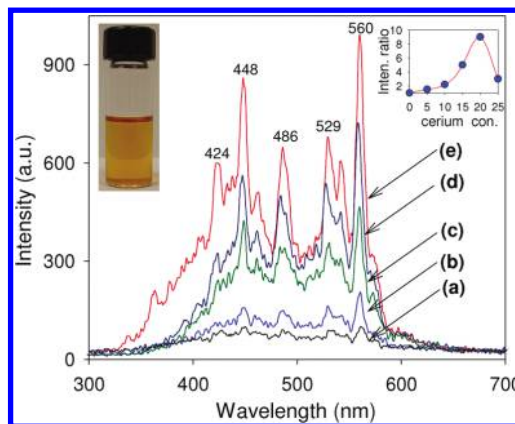
of the defects in crystal structure. The subsequent decrease in emission intensity can be primarily attributed to the increase in particle size of the formed Ce doped $LaCO_3OH$ heterogenerous structure.

To validate our hypothesis, 5.0 mol % copper ion was introduced to $LaCO_3OH$ annular-shaped nanoarchitectures under the same lanthanide doping approach, except that 5.0 mol % $Cu,La(oleate)_3$ complex was used. XRD pattern (Figure 11a) of the as-synthesized Cu doped $LaCO_3OH$ sample shows that there are separate phases: hexagonal $LaCO_3OH$, monoclinic CuO,[44] and cubic Cu_2O[45] phases. No shift of the diffraction peak of the hexagonal $LaCO_3OH$ phase was observed. This demonstrates that the copper ions cannot enter the lattice of $LaCO_3OH$ by occupying the La^{3+} ion sites. They crystallized to form two new separate phases of CuO and Cu_2O dispersing on the $LaCO_3OH$ annular surface. Actually, Cu ion clusters can chemically bond with oxygen ions to form oxide traces on the surface or in the shallow layer of $LaCO_3OH$ annular-shaped nanoarchitectures. The main reason for this was attributed to the radius of La^{3+} ion which is much larger than that of Cu^+ ion ($r(La^{3+}) = 1.172$ Å, $r(Cu^{2+}) = 0.87$ Å, $r(Cu^+) = 0.91$ Å). This is also supported by the SEM image of the 5.0 mol % $Cu/LaCO_3OH$ sample as shown in Figure 11b. It is clearly that the basic morphology of $Cu/LaCO_3OH$ sample is similar to annular shape of undoped $LaCO_3OH$. As evidenced in the TEM image (Figure 11c), 3 nm-sized CuO/Cu_2O particles segregating on the surface of 400 nm-sized $LaCO_3OH$ annular-shaped nanoarchitectures were observed. The segregation of copper(I,II) oxide on the surface of $LaCO_3OH$ nanoarchitectures is probably due to the different decomposition temperature of the Cu- and La-oleate. The different crystallization rates of copper and lanthanum nuclei lead to the formation of heterogenerous structure. Survey XPS spectrum (Supporting Information, S-Figure 5) of this sample also reveals the presence of Cu on the surface layer of annular-shaped nanoarchitectures. The main peak at 932.2 eV belongs to $Cu 2p_{3/2}$, and can be divided into two peaks at 932.2 and 934.6 eV, attributed to Cu^+ and

(41) Pol, V. G.; Thiyagarajan, P.; Moreno, J. M. C.; Popa, M. *Inorg. Chem.* **2009**, *48*, 6417−6424.

(42) Li, G.; Peng, C.; Zhang, C.; Xu, Z.; Shang, M.; Yang, D.; Kang, X.; Wang, W.; Li, C.; Cheng, Z.; Lin, J. *Inorg. Chem.* **2010**, *49*, 10522−10535.

(43) Itoh, T.; Kikkawa, Y.; Biju, V.; Ishikawa, M.; Ikehata, A.; Ozaki, Y. *J. Phys. Chem. B* **2006**, *110*, 21536−21544.

(44) Zhou, H.; Wong, S. S. *ACS Nano* **2008**, *2*, 944−958.

(45) Hung, L. I.; Tsung, C. K.; Huang, W.; Yang, P. *Adv. Mater.* **2010**, *22*, 1−5.
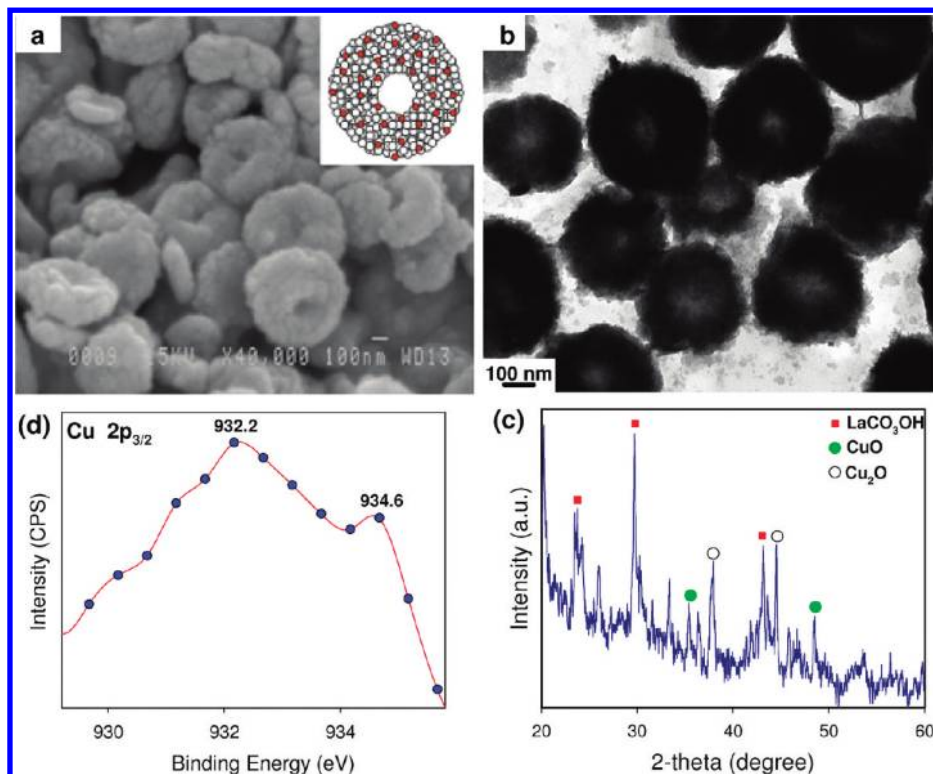
Figure 11. (a) SEM; (b) TEM, inset SAED; (c) XRD; (d) Cu 2p$_{3/2}$ XPS patterns of the as-synthesized Cu/LaCO$_3$OH nanoannulars. Upper inset in (a) shows the simulated structure of a Cu/LaCO$_3$OH annular.
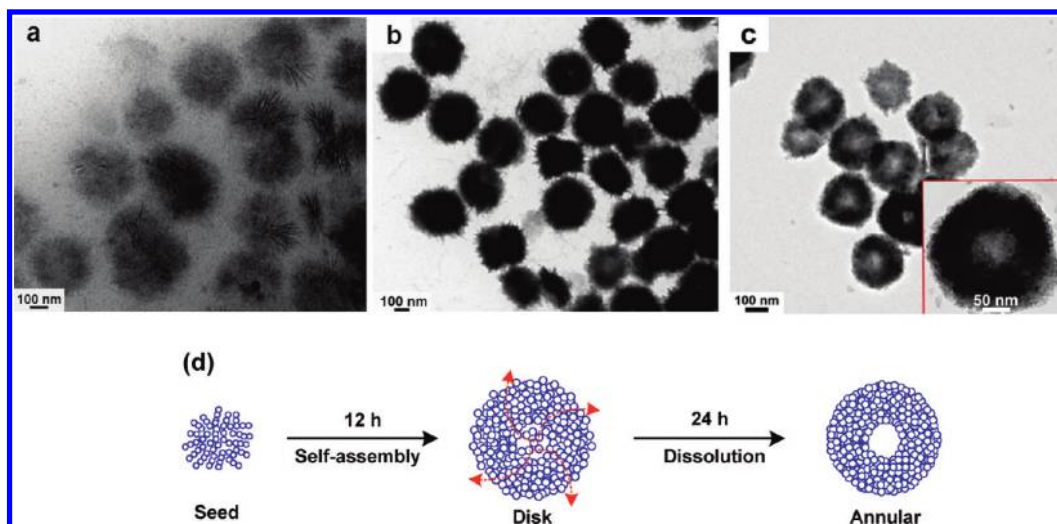

Figure 12. TEM images of 10 mol % cerium doped LaCO$_3$OH samples synthesized at 180 °C with a reaction time of (a) 4 h, (b) 12 h, (c) 24 h. (d) A schematic diagram for the formation of annular-shaped nanoarchitectures.

Cu^{2+}, respectively, corresponding to CuO$_x$,[46] in agreement with the XRD data. The surface composition of the 5.0 mol % Cu/LaCO$_3$OH sample was found to contain 7.3 mol % Cu at the surface. The tendency for excess surface enrichment of copper ions is mainly due to the segregation of copper on the LaCO$_3$OH surface instead of incorporation into the structural lattice.

Because the aggregation is energetically favored, the primary particles tended to aggregate into larger annular-shaped nanoarchitectures to lower the system energies at longer reaction

time. Time-dependent experiments of 10 mol % Ce:LaCO$_3$OH nanoarchitectures were carried out at 180 °C for 4, 12, 24 h. The growth process of the monodisperse homogeneous annular-shaped nanoarchitectures was carefully examined by using TEM. As depicted in Figure 12, some seed aggregates appeared after aging for 4 h (Figure 12a). When the aging time was prolonged to 12 h, these aggregated particles tend to assemble further to form irregular annulars (Figure 12b). They evolved into the perfect 400 nm sized-nanoannulars as the aging time was prolonged to 24 h (Figure 12c). A feasible formation mechanism of the annular-shaped Ce$_x$La$_{1-x}$CO$_3$OH nanoarchitectures is proposed to involve different growth

(46) Sun, X.; Zhang, Y. W.; Si, R.; Yan, C. H. *Small* **2005**, *1*, 1081–1086.

processes as illustrated in Figure 12d. With increased reaction time, more inner $Ce_xLa_{1-x}CO_3OH$ crystals with higher energy gradually dissolved possibly because of the presence of capping oleylamine in homogeneous toluene phase,[47] which finally led to a void space in the center, resulting in mesostructured $Ce_xLa_{1-x}CO_3OH$.

4. Conclusion

In conclusion, mesoporous undoped and cerium doped $LaCO_3OH$ homogeneous annular-shaped nanoarchitectures with large specific surface area have been synthesized through the thermolysis of $Ce_xLa_{1-x}(oleate)_3$ (x = 0−20 mol %) complexes in a toluene−water mixture containing *tert*-buty-lamine/oleylamine at 180 °C for 24 h. The mechanism of the decomposition reaction of $Ce_xLa_{1-x}(oleate)_3$ under catalyz-ing *tert*-butylamine for the formation of $Ce_xLa_{1-x}CO_3OH$ structure and the growth of self-assemblied nanoarchitec-tures are proposed. The conversion of $Ce_xLa_{1-x}CO_3OH$ structure to $Ce_xLa_{1-x}(CO_3)O_2$ at 600 °C, to $Ce_xLa_{1-x}(OH)_3$ at 800 °C, and eventually to $(Ce_xLa_{1-x})_2O_{3-\delta}$ at 900 °C were employed. The XRD results reveal that because cerium and lanthanum have similar ionic radii, the cerium dopant could enter easily into the $LaCO_3OH$ structural lattice. Whereas copper could be unlikely enter into their lattice because of the large ionic radius difference. The XPS results reveal that only one Ce^{3+} oxidation state is in the as-synthesized Ce_x-$La_{1-x}CO_3OH$ samples with doping level ranging from 5 to 15 mol %, whereas both 3+ and 4+ ones coexisted in 20 mol % $Ce:LaCO_3OH$. Upon annealing at high temperatures (800−900 °C) under air atmosphere, the partial conversion of Ce^{3+} into Ce^{4+} occurring on the surface of mixed cerium−lanthanum hydroxide or oxide was observed. The significant luminescence emission intensity of the as-synthesized Ce_x-$La_{1-x}CO_3OH$ samples was found to increase from 1.5 to 9.0 times with increase in cerium dopant concentration from 5 to 20 mol %. This approach was extended to synthesize Cu_2O/CuO doped $LaCO_3OH$ heterogenerous nanoarchitectures. We expect that these mesoporous nanomaterials could offer opportunities for investigating their collective properties and open the door for other technologically important applications.

Supporting Information Available: Further details are given in Figures S-Figure 1 to S-Figure 6. This material is available free of charge via the Internet at http://pubs.acs.org.

(47) An, K.; Kwon, S. G.; Park, M.; Na, H. B.; Baik, S. I.; Yu, J. H.; Kim, D.; Son, J. S.; Kim, Y. W.; Song, I. C.; Moon, W. K.; Park., H. M.; Hyeon, T. *Nano Lett.* **2008**, *8*, 4252–4258.

Two-Phase Synthesis of Colloidal Annular-Shaped $Ce_xLa_{1-x}CO_3OH$ Nanoarchitectures Assemblied from Small Particles and Their Thermal Conversion to Derived Mixed Oxides
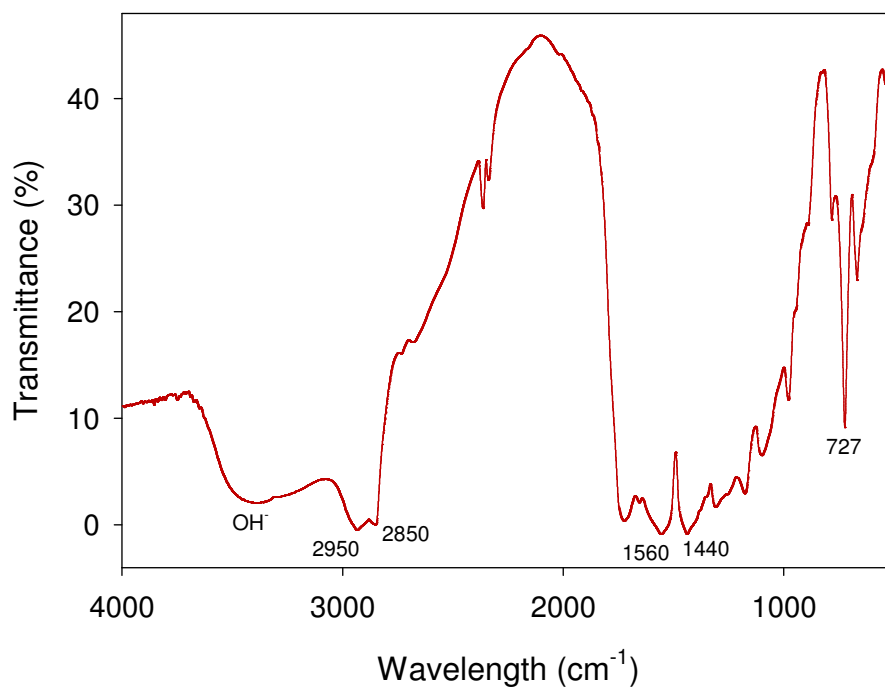
Thanh-Dinh Nguyen, Cao-Thang Dinh, and Trong-On Do[*]

Department of Chemical Engineering, Laval University, Quebec G1K 7P4 Canada

To whom correspondence should be addressed. E-mail: Trong-On.Do@gch.ulaval.ca

Supporting Information

**S-Figure 1.** FTIR spectrum of $Ce_xLa_{1-x}(OA)_3$ complex.

FTIR spectrum of the $Ce_xLa_{1-x}(oleate)_3$ complex solid (after toluene elimination) shows the absorption band at 727 cm^{-1} is assigned to the stretching vibrations of the La-O-Ce bonds. Two absorption bands are observed at 1440 and 1560 cm^{-1}, which are attributed to the symmetric and asymmetric stretching vibrations of the carboxylate groups of oleate ligands, respectively. The absorption bands at 2850 - 2950 cm^{-1} are characteristic of the symmetric and asymmetric methyl and methylene stretches of the alkyl chains.
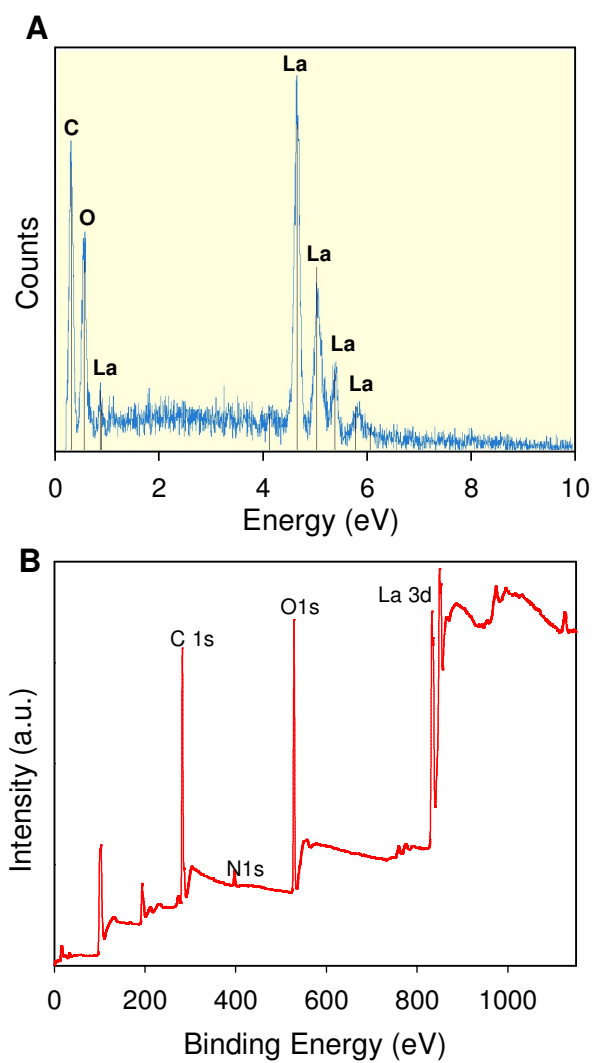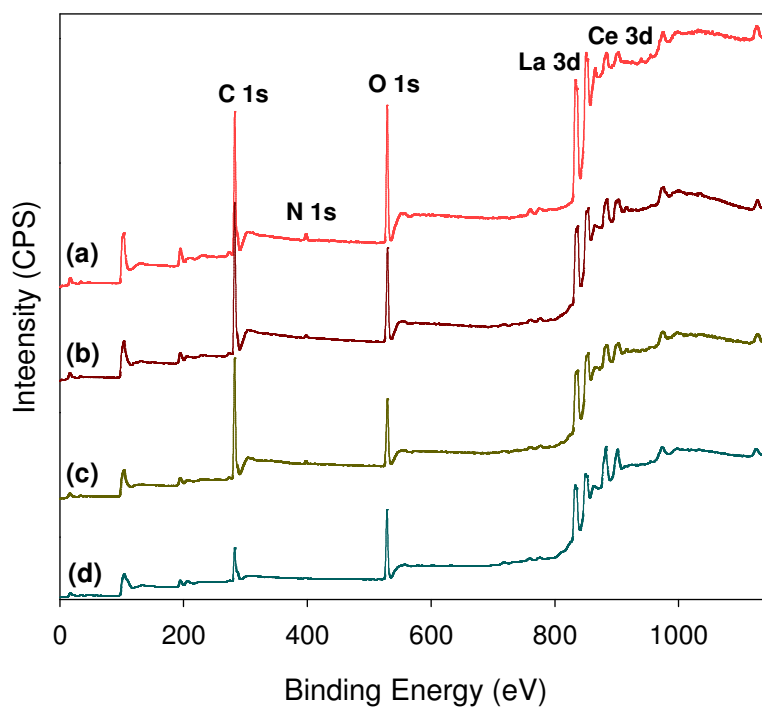
S-Figure 2. (A) EDS and (B) XPS spectra of the as-synthesized $LaCO_3OH$ nanoannulars.
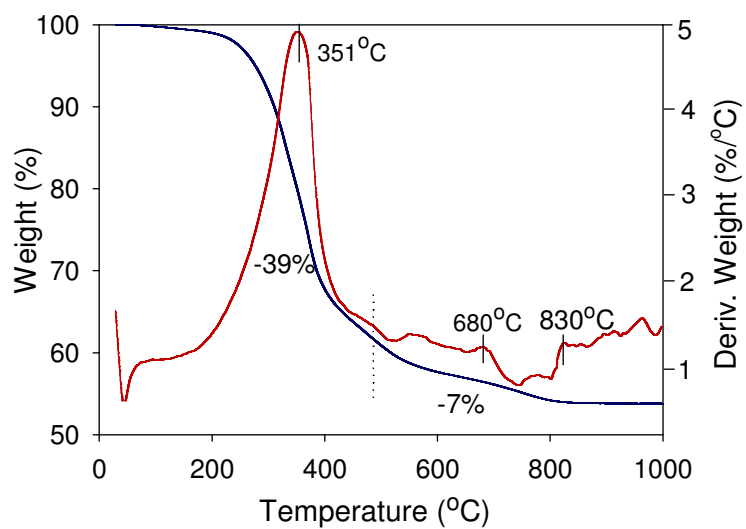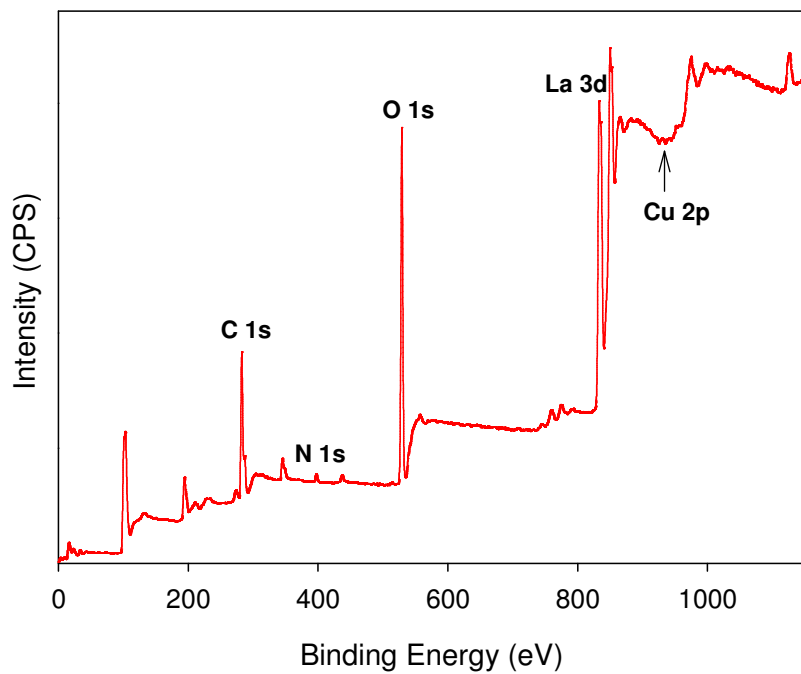
S-Figure 3. TGA-DTA curves of the as-synthesized oleylamine-capped Cerium-doped LaCO$_3$OH nanoannulars.
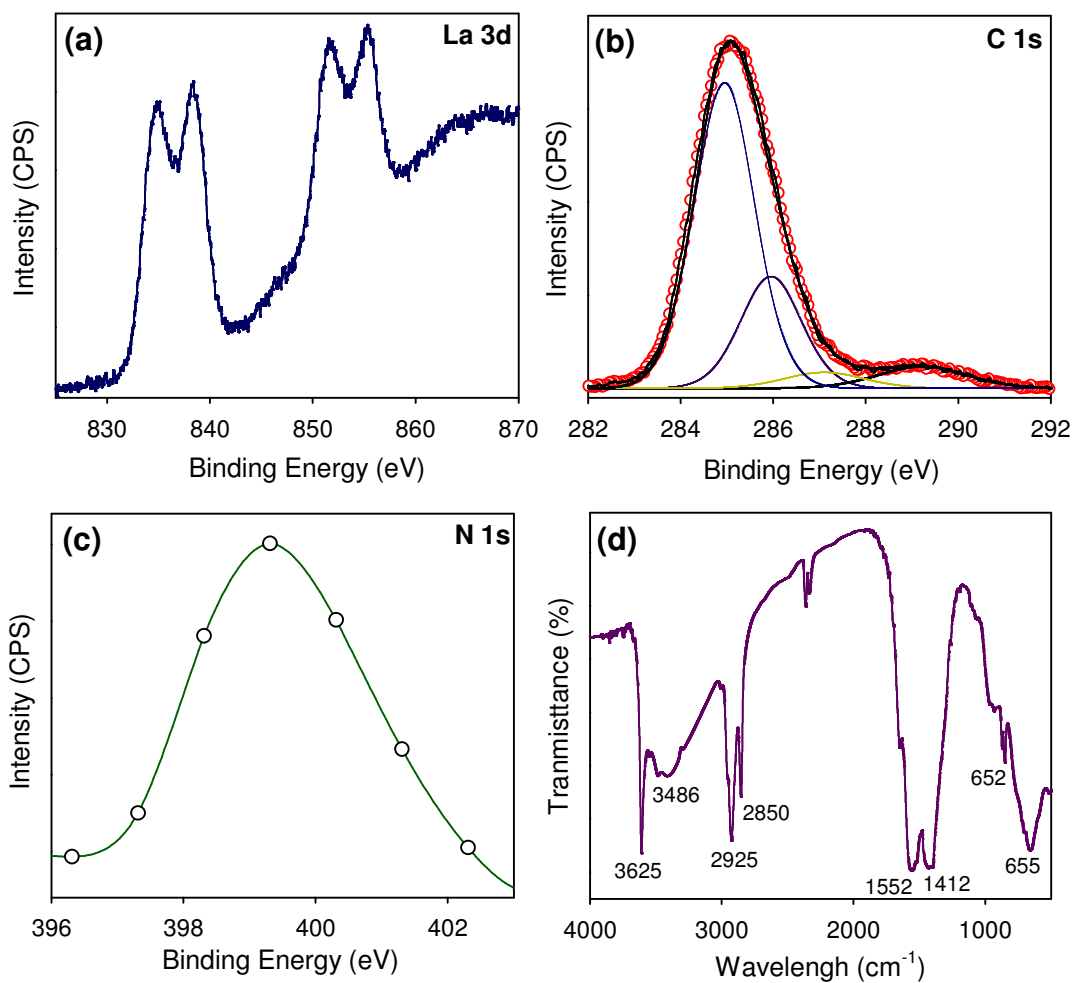
S-Figure 4. (a) La 3d; (b) N 1s; (c) C 1s XPS; (d) FTIR spectra of the as-synthesized 10 mol% cerium doped LaCO$_3$OH nanoannulars.

S-Figure 5. Survey XPS spectra of the as-synthesized $LaCO_3OH$ with various cerium concentration (mol%): (a) $x = 5$; (b) $x = 10$; (c) $x = 15$; (d) $x = 20$.

S-Figure 6. Survey XPS spectrum of the as-synthesized Cu/LaCO$_3$OH heterogenerous nanoannulars.